How to cite: Angew. Chem. Int. Ed. 2024, e202319853
doi.org/10.1002/anie.202319853

Bioorthogonal Chemistry

Tetrazine-Isonitrile Bioorthogonal Fluorogenic Reactions Enable Multiplex Labeling and Wash-Free Bioimaging of Live Cells

Yingqiao Deng[+], Tianruo Shen[+], Xinyu Yu[+], Jie Li, Peixuan Zou, Qiyong Gong, Yongxiang Zheng, Hongbao Sun, Xiaogang Liu,* and Haoxing Wu**

Abstract: Developing fluorogenic probes for simultaneous live cell labeling of multiple targets is crucial for understanding complex cellular events. The emerging [4+1] cycloaddition between tetrazine and isonitriles holds promise as a bioorthogonal tool, yet existing tetrazine probes lack reactivity and fluorogenicity. Here, we present the development of a series of tetrazine-functionalized bioorthogonal probes. By incorporating pyrazole adducts into the fluorophore scaffolds, the post-reacted probes displayed remarkable fluorescence turn-on ratios, up to 3184-fold. Moreover, these modifications are generalizable to various fluorophores, enabling a broad emission range from 473 to 659 nm. Quantum chemical calculations further elucidate the turn-on mechanisms. These probes enable the simultaneous labeling of multiple targets in live cells, without the need for a washing step. Consequently, our findings pave the way for advanced multiplex imaging and detection techniques for cellular studies.

Bioorthogonal fluorogenic probes have become crucial tools for intracellular and in vivo imaging.[1] These probes emit fluorescence exclusively upon bioorthogonal reactions, which greatly enhances signal-to-noise ratios by minimizing background interference.[2] While numerous probes have been developed, many are restricted to specific reactions, like the inverse electron-demand Diels–Alder (IEDDA) reactions between tetrazine and dienophiles (Figure 1A).[3] Alternative bioorthogonal fluorogenic strategies, which maintain mutual orthogonality to IEDDA reactions, are limited.[4] This restriction hampers applications that neces-

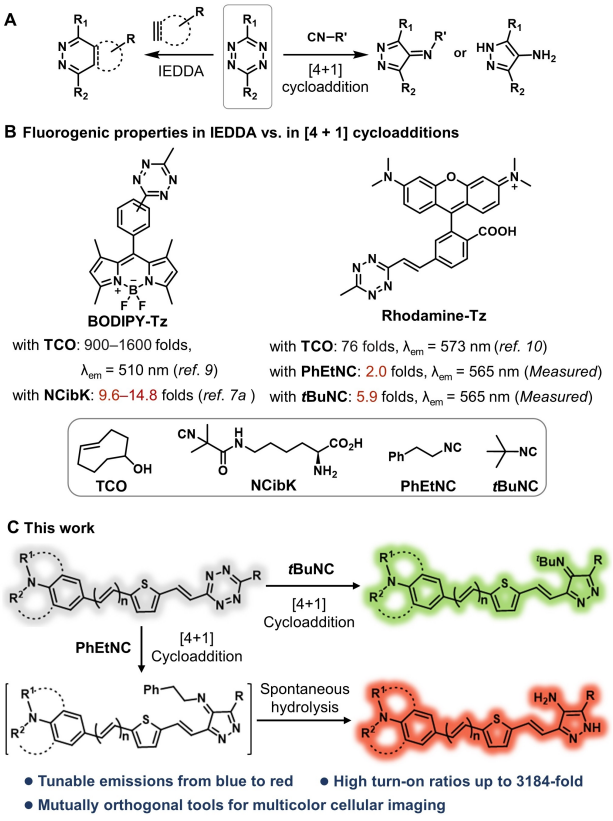

Figure 1. A) Schematic illustration of tetrazine bioorthogonal reactions: IEDDA reactions (left) and [4+1] cycloadditions (right). B) Comparison of fluorogenic properties of reported tetrazine probes between IEDDA reactions and [4+1] cycloadditions. C) Schematic illustration of in situ fluorophore formation strategy via tetrazine-isonitrile chemistry.

[*] Y. Deng,[+] X. Yu,[+] J. Li, Prof. Q. Gong, Prof. H. Sun, Prof. H. Wu
Department of Radiology and Huaxi MR Research Center (HMRRC), Functional and Molecular Imaging Key Laboratory of Sichuan Province and Frontiers Science Center for Disease Related Molecular Network
West China Hospital, Sichuan University
Huaxi Research Building, 001 4th Keyuan Road, 610041, Chengdu (China)
E-mail: hongbaosun@scu.edu.cn
haoxingwu@scu.edu.cn

T. Shen,[+] Prof. X. Liu
Science, Mathematics and Technology Cluster
Singapore University of Technology and Design
8 Somapah Road, 487372, Singapore (Singapore)
E-mail: xiaogang_liu@sutd.edu.sg

P. Zou, Prof. Y. Zheng
Department of Biopharmaceutics
West China School of Pharmacy, Sichuan University
No.17 People's South Road, 610041, Chengdu (China)

P. Zou, Prof. Y. Zheng, Prof. H. Wu
Key Laboratory of Drug-Targeting and Drug Delivery System of the Education Ministry
Sichuan Engineering Laboratory for Plant-Sourced Drug and Sichuan Research Center for Drug Precision Industrial Technology
West China School of Pharmacy, Sichuan University
No.17 People's South Road, 610041, Chengdu (China)

[+] These authors contributed equally to this work.

sitate the simultaneous labeling of multiple targets or the detection of their interactions within a single live cell.[5]

The recently discovered [4+1] cycloaddition reactions between tetrazine and isonitriles, resulting in pyrazole adduct formation, offer a distinct alternative to IEDDA reactions (Figure 1A).[6] This cycloaddition reaction has garnered significant attention for protein labeling and drug delivery due to its excellent biocompatibility, rapid kinetics, and good payload release.[6b,7] Interestingly, introducing a bulky substituent (e.g., *tert*-butyl) to tetrazine preserves its reactivity with isonitriles while reducing it towards dienophiles,[7b,8] establishing [4+1] cycloaddition as orthogonal to IEDDA and other bioorthogonal chemistries.[5,7e]

Despite these benefits, the fluorogenicity of isonitrile-tetrazine chemistry has been underwhelming. Previous research reveals that fluorogenic BODIPY-tetrazine probes exhibit only modest turn-on ratios upon reacting with isonitrile derivatives.[7a] This contrasts significantly with the two-order-of-magnitude fluorescence enhancement seen in IEDDA reactions (Figure 1B).[9] Our in-house measurements using rhodamine fluorophores[10] further confirmed the limited fluorogenicity of existing tetrazine-isonitrile chemistry (Figure 1B; Figure S1). Novel design strategies are thus imperative to unlock the fluorogenic potential of this chemistry for biological applications.

In this study, we introduced an in situ formation strategy, merging pyrazole and fluorophores into a unified π-conjugated system, deviating from the conventional approach of isolating their π-conjugations (Figure 1C). Building on our established Huaxi-Fluors framework,[11] we synthesized a diverse series of tetrazine-based probes. Upon bioorthogonal reaction with isonitriles, these probes showcased remarkable fluorescence turn-on ratios (up to 3184-fold), accompanied by tunable emission wavelengths (473–659 nm). Quantum chemical calculations offered insights into the unique fluorescence turn-on mechanism of these new probes. Finally, we showcased the mutually orthogonal reactivity of these probes with respect to IEDDA and other classical bioorthogonal reactions, allowing for simultaneous wash-free imaging of multiple subcellular targets in live cells.

To evaluate our molecular design strategy, we initially synthesized and examined the fluorescence turn-on effect of probe **1/HF$_{642}$** with 2-phenylethyl isonitrile (**PhEtNC**, Figure 2A), resulting in the formation of the aminopyrazole adduct through a [4+1] cycloaddition and a spontaneous hydrolysis process. Encouragingly, aminopyrazole (**aP1**), exhibited remarkable fluorescence turn-on ratios of 294-fold in ethanol (EtOH) and 537-fold in PBS, respectively (Figure 2B; Table S1). These ratios exceeded those of previous tetrazine-isonitrile chemistry by one or two orders of magnitude. Moreover, the intramolecular charge transfer feature of **aP1** led to a significant redshift of peak emission wavelength (λ_{em}) from 536 nm in EtOH to 615 nm in PBS. Despite its favorable λ_{em}, **aP1** demonstrated relatively low brightness due to limited solubility and aggregation-caused quenching (Figure 2B; Table S1).

Subsequently, we aimed to optimize probe fluorogenicity and enrich color choices by designing and synthesizing

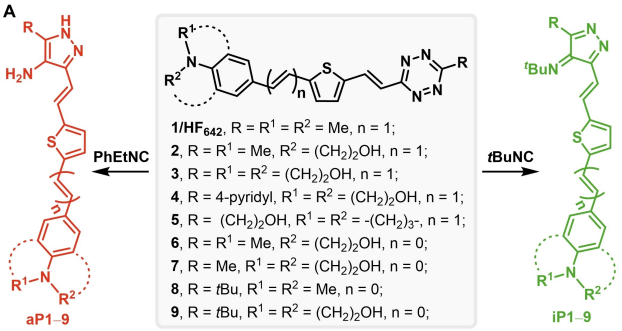

B

Probe	With **PhEtNC**					With ***t*BuNC**				
	λ_{em} [nm]	ε × 10^4	Turn-on	Φ	$\varepsilon\Phi$ × 10^4	λ_{em} [nm]	ε × 10^4	Turn-on	Φ	$\varepsilon\Phi$ × 10^4
1	615	0.82	537	0.12	0.10	562	0.37	44	0.03	0.01
2	613	1.10	550	0.15	0.17	556	0.61	49	0.09	0.05
3	601	2.64	1170	0.17	0.45	550	1.22	99	0.17	0.21
4	620	0.52	368	0.03	0.02	592	0.73	23	0.002	0.001
5	659	0.99	255	0.02	0.02	607	1.15	100	0.004	0.005
6	551	3.15	601	0.42	1.32	519	1.43	100	0.07	0.10
7	546	4.41	887	0.34	1.50	513	2.09	679	0.13	0.27
8	554	2.49	555	0.24	0.60	550	0.26	48	0.06	0.02
9	542	2.50	1705	0.39	0.98	533	0.32	236	0.37	0.11

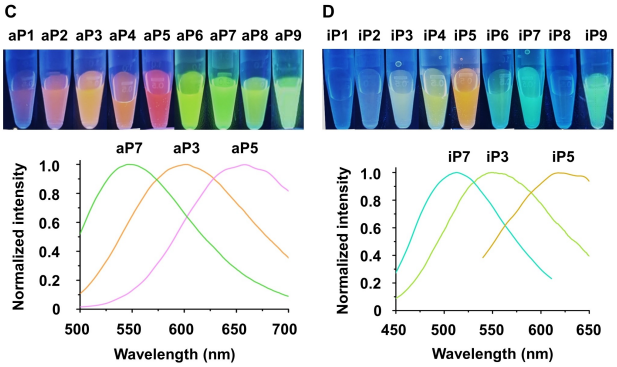

Figure 2. A) Molecular structures of Huaxi-Fluor probes and their products after reacting with two isonitriles. B) Photophysical properties of Huaxi-Fluor probes in PBS after reacting with **PhEtNC** or ***t*BuNC**, including peak emission wavelengths (λ_{em}), maximum molar extinction coefficients (ε, $M^{-1}cm^{-1}$), fluorescence turn-on ratios, quantum yields (Φ), and brightness ($\varepsilon\Phi$, $M^{-1}cm^{-1}$) of bioorthogonal products. Physical appearances of C) (top) **aP1**–**aP9** and D) (top) **iP1**–**iP9** (10 μM) in PBS under the exposure of an ultraviolet excitation lamp of 365 nm. Compounds **aP4**, **iP4**, **aP5**, and **iP5** are diluted in PBS/DMSO (7:3). Emission spectra of representative probes after reacting with C) (bottom) **PhEtNC** and D) (bottom) ***t*BuNC** in PBS.

probes **2**–**9** based on the frameworks of Huaxi-Fluors, varying conjugation lengths and solubilities. These probes generated two types of conjugated products, aminopyrazole and iminopyrazole ligations, upon tetrazine-isonitrile bioorthogonal reactions with substrates **PhEtNC** and ***t*BuNC** (Figure 2A). This allowed us to comprehensively explore the structure–property relationship of these probes in their reactions with **PhEtNC** and ***t*BuNC**. Successful reactions of all probes with **PhEtNC** resulted in highly fluorogenic biorthogonal adducts, **aP2**–**aP9**. These products exhibited substantial Stokes shifts (up to 239 nm) and diverse

fluorescence turn-on ratios ranging from 140-fold to 3184-fold (Figure 2B; Table S1). Additionally, by altering π-conjugation lengths or introducing various substituents, we achieved tunable λ_{em} values from 542 nm to 659 nm in PBS (Figures 2B–2D).

Notably, solubility significantly influenced the brightness of aminopyrazoles, especially in aqueous solutions (Figure 2C). For instance, probe **3** with hydrophilic substituents displayed improved solubility and the highest brightness ($0.45\times10^4\ M^{-1}cm^{-1}$) in PBS, nearly three to four times higher than probes **1** and **2**. Similarly, green fluorescence probes **6**–**9** exhibited excellent molar extinction coefficients and quantum yields, resulting in high brightness levels of up to $1.50\times10^4\ M^{-1}\ cm^{-1}$ upon reacting with **PhEtNC**. These values rival the performance of several commercially available dyes.[12]

Upon interaction with ***t*BuNC**, the resultant iminopyrazole products **iP1**–**iP9** demonstrated fluorescence turn-on ratios of 23 to 1035-fold in both EtOH and PBS. These substantial turn-on ratios make them suitable for wash-free cell imaging. Similar to aminopyrazoles, consistent structure–property relationships emerged, regarding the impact of π-conjugation and solubility on iminopyrazole fluorescent properties. However, in contrast to aminopyrazole products, the corresponding iminopyrazoles consistently exhibited a blue shift in λ_{em} (by ~40 nm). Molar extinction coefficients (ε) and brightness ($\varepsilon\Phi$) were also relatively lower for these iminopyrazole analogies (Figure 2B; Table S1).

We subsequently conducted comprehensive density functional theory (DFT) and time-dependent density functional theory (TD-DFT) calculations[13] to understand the distinct fluorescent characteristics exhibited by aminopyrazoles and iminopyrazoles (Figure 3A, 3B). Our findings reveal that probe **3** exhibits minimal emission due to a low-lying dark state (S_1, $f=0.0052$) originating from the tetrazine fragment during the photoexcitation (Figure 3A left). Above this dark state, a bright state (S_2, $f=1.7644$) emerges, driven by the π–π* transition spanning the scaffold of the whole probe. This bright state is primarily responsible for ultraviolet-visible (UV/Vis) light absorption (Figure 3A left). As a consequence, energy absorbed by S_2 transfers to the dark S_1 through internal conversion,[14] leading to fluorescence quenching in the precursor. Conversely, after the [4+1] cycloaddition reactions with **PhEtNC** and subsequent hy-

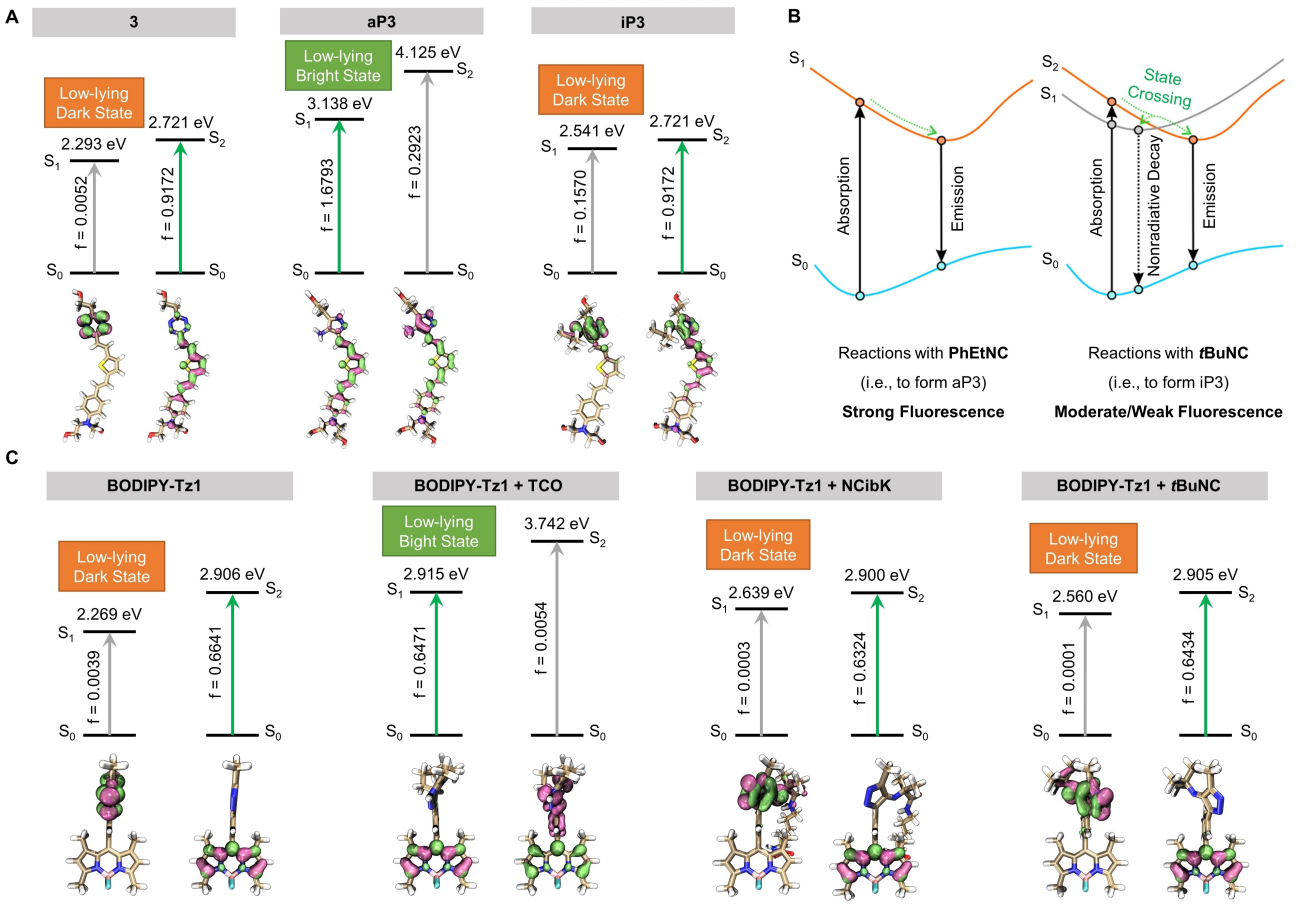

Figure 3. A) Energy levels of different states of probe **3** (left), **aP3** (middle), and **iP3** (right) during the vertical excitation progress. The bottom panel illustrates the hole-electron distributions during the vertical excitation (pink: hole, green: electron). B) Schematic illustrations of the fluorescence mechanisms of Huaxi-Fluors after reacting with **PhEtNC** and ***t*BuNC**. C) Energy levels of different states of **BODIPY-Tz1**, **BODIPY-Tz1 + TCO**, **BODIPY-Tz1 + NCibK**, and **BODIPY-Tz1 + *t*BuNC** during the vertical excitation progress. The bottom row demonstrates the hole-electron distributions during the vertical excitation (pink: hole, green: electron).

drolysis, the dark state vanishes in the aminopyrazole product (**aP3**). The newly generated S_1 stems from the π–π* transition distributed throughout the entire probe, with a substantial *f* value of 1.6793 (Figure 3A). This bright state remains stabilized upon geometric relaxation ($f=1.7378$; Figure S51), resulting in a pronounced fluorescence turn-on ratio. In comparison, the reaction with ***t*BuNC** yields a stable "dimmed" state (S_1) in the iminopyrazole product **iP3** characterized by a reduced *f* value (0.1570). This is attributed to the strong contribution from the n-π* transition of the newly formed *4H*-pyrazol-4-imine fragment (Figure 3A; Figure S56b). The bright S_2 is only 0.180 eV higher than the "dimmed" S_1. Upon geometry relaxation, the bright state becomes stabilized, emitting considerable fluorescence. However, the n-π* transition of the 4H-pyrazol-4-imine fragment could still partially quench its fluorescence and compromise its quantum yield (Figure 3B). These observations suggest that **iP3** exhibits moderate or weak turn-on ratios. A similar pattern emerged in the other four Huaxi-Fluor molecules (Figures S47–S56).

We also compared fluorescence quenching mechanisms with previously reported tetrazine chemistry. For instance, the fluorescence quenching of **BODIPY-Tz1** follows the energy transfer to a dark state (ETDS)[3c] model (Figure 3C; Figures S44, S45). During the vertical excitation of **BODIPY-Tz1**, the UV/Vis absorption is induced by the bright S_2 ($f=0.6641$), which is dominated by the π–π* transition on the **BODIPY** fragment. Below this state, a stabilized dark S_1 is observed. This state involves n-π* transition localized in the tetrazine group with a negligible *f* value (0.0039). Consequently, **BODIPY-Tz1** emits minimal fluorescence after photoexcitation due to efficient energy transfer from BODIPY (S_2, a bright state) to tetrazine (S_1, a dark state). Upon the IEDDA reaction, the tetrazine moiety is eliminated by *trans*-cyclooctene (TCO), eradicating the prior dark S_1 and ensuring a new bright S_1 ($f=0.6471$) in the **BODIPY-Tz1+TCO**. This bright state primarily results from the π–π* transition of the BODIPY segment, facilitating fluorescence recovery ($\varphi=0.8$). Conversely, **BODIPY-Tz1+NCibK** derived from the reaction between **BODIPY-Tz1** and **NCibK** retains a stabilized dark state (S_1, $f=0.0003$). This dark state arises from the forbidden n-π* transition within the *4H*-pyrazol-4-imine fragment. As a result, **BODIPY-Tz1+NCibK** remains weakly emissive with a low fluorescence turn-on ratio. Comparable results were also found in the resultant (**BODIPY-Tz1+*t*BuNC**) produced from the reaction with ***t*BuNC**. Similar calculations were executed on **BODIPY-Tz2**, an isomer of **BODIPY-Tz1**, along with its biorthogonal derivatives, i.e., **BODIPY-Tz2+TCO** and **BODIPY-Tz2+NCibK** (Figures S44, S46). These consistent computational results rationalize our newly discovered tetrazine-isonitrile chemistry's superior fluorogenicity in comparison to tetrazine-**NCibK** reactions, by modifying the residue moiety after bioorthogonal reactions and removing the low-lying dark state.

Subsequently, we explored the bioorthogonal kinetics and stability of our tetrazine-based probes to evaluate their potential for fluorescence imaging applications. Conducted under DMSO/PBS buffer conditions (2:3, pH 7.4) at 37 °C, we determined the rate constant of probe **4** towards ***t*BuNC** as 0.231 $M^{-1}s^{-1}$ (Figure S21). These values, consistent with previous reports,[7a,b] are deemed suitable for live cell labeling. Furthermore, probe **9** demonstrated robust stability in maintaining its fluorescence turn-on efficiency through the [4+1] cycloaddition with isonitriles in culture media over several hours (Figures S23, S24). Additionally, we investigated the cytotoxicity of probes **9**, **11**, and **12** and their bioorthogonal reaction products (Figures S25–S29). CCK8 assay results indicated that both the probes and their iminopyrazole adducts showed negligible cytotoxicity against SKOV3 cells and embryonic kidney cells (293T cells). After 24 hours of incubation, cell viability remained consistently above 92 %.

To further assess the applicability of our newly developed fluorogenic probes in live-cell imaging, we designed and synthesized three *tert*-butyl isonitrile derivatives. These include chloroalkane isonitrile ligand **10**, for labeling intracellular HaloTag-fusion proteins, as well as two small-molecule compounds, **11** and **12**, intended for targeting endoplasmic reticulum (ER) and lysosome, respectively (Figure 4E). Initially, we transiently transfected 293T cells with nucleus-targeting constructs to express Halo-EBFP2-H2A. Subsequently, cells were pretreated with ligand **10**, followed by incubation with probe **9** for one hour. Without a washing step, we imaged the cells using confocal microscopy and observed specific labeling in the nucleus (Figure 4A). This labeling showed good colocalization with the blue channel, indicating potent protein expression. Conversely, control groups lacking treatment with the HaloTag isonitrile ligands exhibited negligible signals (Figures S35, S43).

Similarly, after incubating the SKOV3 cell line with probe **9** for an hour, followed by incubation with **11** or **12** without washing, a significant increase in fluorescence pixel intensity (up to 196-fold relative to surrounding areas, Figure 4B, 4C; Figures S32, S33) was observed in the ER or lysosomal. This signal colocalized with the corresponding ER-tracker or Lyso-tracker Red, demonstrating a marked signal-to-background contrast. Conversely, control groups lacking isonitrile treatment exhibited negligible signals with an ~18.6-fold lower pixel intensity (Figure 4D; Figure S34).

We extended the highly fluorogenic tetrazine-isonitrile chemistry as a mutually orthogonal tool, alongside other bioorthogonal strategies such as Copper(I)-catalysed azide-alkyne cycloaddition (CuAAC), strain-promoted azide-alkyne cycloadditions (SPAAC), and IEDDA reactions, for multiplexed labeling and detection applications. In this context, we first assessed the orthogonality of tetrazine-isonitrile reaction with other bioorthogonal reactions in solution. Encouragingly, liquid chromatography-mass spectrometry (LC–MS) detection showed that **1**, **9**, or azide exclusively react with the corresponding biorthogonal partners, respectively, without the formation of detectable cross-reactive products (Figure 5A; Figures S36–S39). Dual-color protein labeling was efficiently achieved using dibenzocyclooctyne (DBCO)-fluorophore conjugates (**AF647-DBCO**) and the Huaxi-Fluors scaffold by modulating π-conjugate bridge lengths and substituents. Bovine serum albumin (BSA) was modified with ***t*BuNC**, and Cetuximab

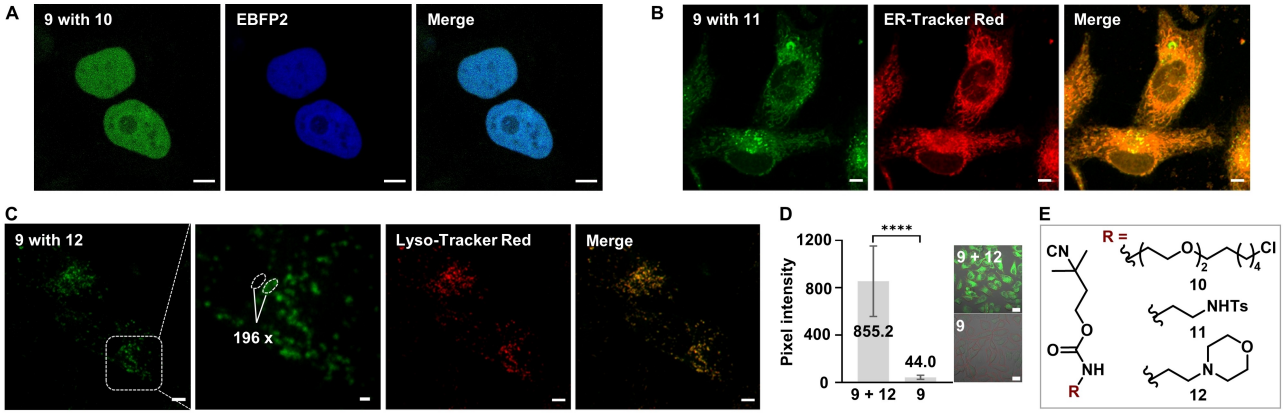

Figure 4. No-wash subcellular imaging in live cells using probe **9**. A) Confocal images of 293T cells, with the nucleus expressing Halo-EBFP2-H2A labeled with **10** (2 μM), followed by [4+1] cycloaddition with probe **9** (100 μM) for 1 hour. B, C) Confocal images of SKOV3 cells treated with probe **9** (1 μM) and the corresponding isonitrile (100 μM) **11** (B) or **12** (C) and comparison of pixel intensity between regions of interest within and outside of lysosomal. Scale bar: 5 μm. D) Semi-quantification and statistical analysis of fluorescence (Excitation, 405 nm; Emission, 520–600 nm) in live SKOV3 cells treated with probe **9** alone or in combination with isonitrile **12**. Error bars indicate mean ± SD ($n = 150$ cells, from 5 images across three independent experiments). Significance differences between the two groups were evaluated using Student's t-test, with ****$P \leq 0.0001$. The scale bar corresponds to 20 μm. E) Chemical structures of tert-butyl isonitrile derivatives.

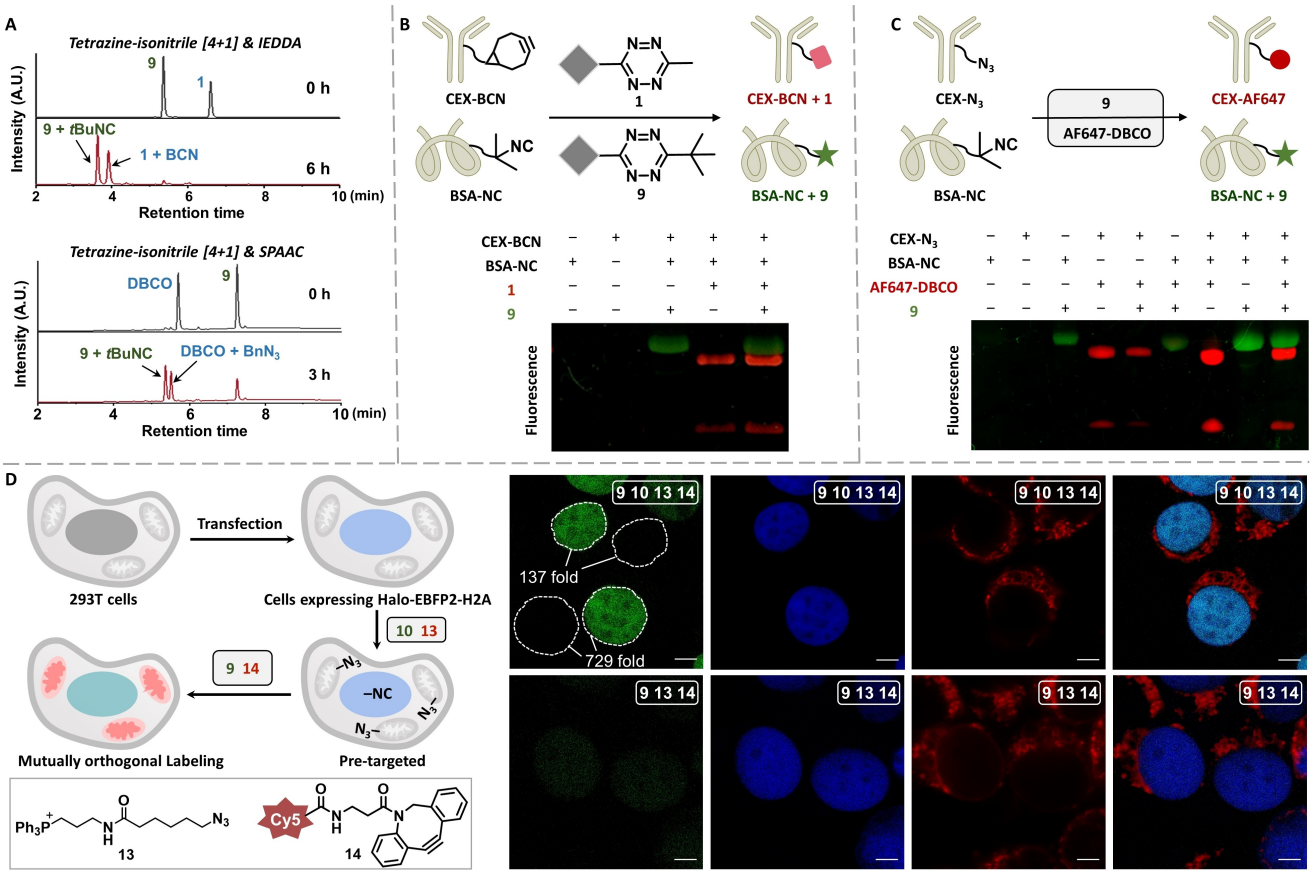

Figure 5. A) Mutually orthogonal bioorthogonal reactions involving tetrazine-isonitrile [4+1] reactions, IEDDA reactions, or SPAAC reactions monitored by LC–MS. B, C) Schematic illustration and in-gel fluorescence analysis of the protein dual labeling using the orthogonal tetrazine-isonitrile [4+1] and IEDDA reactions (B) or SPAAC reactions (C). D) No-wash multicolor labeling for distinct subcellular targets and comparison of pixel intensity between regions of interest within and outside of nucleus. The transfected 293T cells were incubated with **10** (2 μM), and **13** (10 μM), followed by the addition of probe **9** (100 μM), and probe **14** (200 nM) at 37 °C for 1 h. The cells were then imaged by a confocal laser scanning microscope. Scale bar: 5 μm.

(CEX) was decorated with azide or BCN, respectively. Subsequent incubation of these protein conjugates with probes **9** and **1** or **AF647-DBCO**, individually or simultaneously, was performed with in-gel fluorescence, confirming the compatibility of these mutually orthogonal tools with biomolecular labeling, free from cross-reactive artifacts (Figure 5B, 5C; Figures S40, S41).

Lastly, we applied these tools to label distinct subcellular targets within a single living cell. Focusing on the nucleus-located proteins and mitochondria, we incubated the above-mentioned 293T cells, which express Halo-EBFP2-H2A, with ligand **10** and azide **13** for 30 minutes, followed by the addition of tetrazine probe **9** and DBCO probe **14** at 37 °C for an hour (Figure 5D). Subsequent imaging of 293T cells, without washing steps, using a confocal laser scanning microscope unveiled robust green fluorescence from the nucleus in Halo-EBFP2 expression-positive cells, with an S/N ratio up to 700-fold (Figure 5D; Figure S43). Meanwhile, we observed vivid mitochondria stains in the red channel with negligible inter-organelle cross-staining. Similarly, when we incubated SKOV3 cells with probes **4**, **9**, and two targeting molecules (**11** and **S29**), we successfully observed orthogonal labeling in the membrane (PM) and ER (Figure S42). These findings underscore the capability of tetrazine-isonitrile bioorthogonal chemistry to function as mutually orthogonal tools, enabling simultaneous and precise labeling of multiple targets in live cell environments.

In summary, by harnessing the in situ fluorophore generation strategy, we developed a series of highly effective fluorogenic probes based on the tetrazine-isonitrile bioorthogonal chemistry. These probes yield pyrazole adducts via either ligation or dissociation reactions, both displaying exceptional fluorogenic properties, including remarkable turn-on ratios (up to ~3184-fold) and a tunable emission range spanning 473 to 659 nm. Our quantum chemical calculations have illuminated the role of reaction residues and associated dark states in modulating the fluorescence turn-on ratio. Furthermore, these probes demonstrate favorable biocompatibility and orthogonal compatibility with other bioorthogonal chemistries, making them ideally suited for simultaneous live-cell labeling of multiple intracellular targets without the necessity for washing steps. We believe that our research significantly contributes to the arsenal of bioorthogonal fluorogenic imaging tools in multiplex labeling and detection endeavors.

Acknowledgements

This work was supported by the National Key R&D Program of China (2022YFC2009902, 2002YFC2009900), the National Natural Science Foundation of China (21977075, 22271200), the Natural Science Foundation of Sichuan, China (2023NSFSC1716), the 1·3·5 Project for Disciplines of Excellence at West China Hospital, Sichuan University (ZYYC23003), Agency for Science, Technology and Research (A*STAR, Singapore) under its Advanced Manufacturing and Engineering Program (A2083c0051), and SUTD Kickstarter Initiative (SKI 2021_01_01). We thank Feijing Su and Qifeng Liu at the Core Facilities of West China Hospital and Xiaoyan Wang and Yuanming Zhai at the Analytical & Testing Center of Sichuan University for their help with NMR measurements. We thank Qianlun Pu and Fei Fu at the Advanced Mass Spectrometry Center of West China Hospital for their help with HRMS measurements.

Conflict of Interest

The authors declare no conflict of interest.

Data Availability Statement

The data that support the findings of this study are available in the supplementary material of this article.

Keywords: bioorthogonal chemistry · cycloadditions · pyrazole · fluorophores · dark state

[1] a) S. L. Scinto, D. A. Bilodeau, R. Hincapie, W. Lee, S. S. Nguyen, M. Xu, C. W. am Ende, M. G. Finn, K. Lang, Q. Lin, J. P. Pezacki, J. A. Prescher, M. S. Robillard, J. M. Fox, *Nat. Rev. Methods Primers* **2021**, *1*, 30; b) T. Cañeque, S. Müller, R. Rodriguez, *Nat. Chem. Rev.* **2018**, *2*, 202–215; c) N. K. Devaraj, *ACS Cent. Sci.* **2018**, *4*, 952–959.

[2] P. Shieh, C. R. Bertozzi, *Org. Biomol. Chem.* **2014**, *12*, 9307–9320.

[3] a) H. Wu, N. K. Devaraj, *Acc. Chem. Res.* **2018**, *51*, 1249–1259; b) B. L. Oliveira, Z. Guo, G. J. L. Bernardes, *Chem. Soc. Rev.* **2017**, *46*, 4895–4950; c) W. Chi, L. Huang, C. Wang, D. Tan, Z. Xu, X. Liu, *Mater. Chem. Front.* **2021**, *5*, 7012–7021.

[4] T. K. Heiss, R. S. Dorn, A. J. Ferreira, A. C. Love, J. A. Prescher, *J. Am. Chem. Soc.* **2022**, *144*, 7871–7880.

[5] a) S. S. Nguyen, J. A. Prescher, *Nat. Chem. Rev.* **2020**, *4*, 476–489; b) V. Rigolot, C. Biot, C. Lion, *Angew. Chem. Int. Ed. Engl.* **2021**, *60*, 23084–23105; *Angew. Chem.* **2021**, *133*, 23268–23289.

[6] a) H. Stöckmann, A. A. Neves, S. Stairs, K. M. Brindle, F. J. Leeper, *Org. Biomol. Chem.* **2011**, *9*, 7303–7305; b) J. Tu, M. Xu, S. Parvez, R. T. Peterson, R. M. Franzini, *J. Am. Chem. Soc.* **2018**, *140*, 8410–8414.

[7] a) Y. Chen, K.-L. Wu, J. Tang, A. Loredo, J. Clements, J. Pei, Z. Peng, R. Gupta, X. Fang, H. Xiao, *ACS Chem. Biol.* **2019**, *14*, 2793–2799; b) J. Tu, D. Svatunek, S. Parvez, A. C. Liu, B. J. Levandowski, H. J. Eckvahl, R. T. Peterson, K. N. Houk, R. M. Franzini, *Angew. Chem. Int. Ed. Engl.* **2019**, *58*, 9043–9048; *Angew. Chem.* **2019**, *131*, 9141–9146; c) J. Tu, D. Svatunek, S. Parvez, H. J. Eckvahl, M. Xu, R. T. Peterson, K. N. Houk, R. M. Franzini, *Chem. Sci.* **2020**, *11*, 169–179; d) M. Xu, T. Deb, J. Tu, R. M. Franzini, *J. Org. Chem.* **2019**, *84*, 15520–15529; e) X. Zhang, H. Xu, J. Li, D. Su, W. Mao, G. Shen, L. Li, H. Wu, *Chem. Commun.* **2022**, *58*, 573–576; f) Á. Szatmári, G. B. Cserép, T. Molnár, B. Söveges, A. Biró, G. Várady, E. Szabó, K. Németh, P. Kele, *Molecules* **2021**, *26*, 4988; g) H. Ji, W. Xiong, S. Guo, S. Wang, X. Xing, T. Tian, X. Zhou, *ACS Chem. Biol.* **2023**, *18*, 1829–1837; h) D. Svatunek, K. Chojnacki, T. Deb, H. Eckvahl, K. N. Houk, R. M. Franzini, *Org. Lett.* **2023**, *25*, 6340–6345.

[8] T. Deb, R. M. Franzini, *Synlett* **2020**, *31*, 938–944.

[9] J. C. T. Carlson, L. G. Meimetis, S. A. Hilderbrand, R. Weissleder, *Angew. Chem. Int. Ed. Engl.* **2013**, *52*, 6917–6920; *Angew. Chem.* **2013**, *125*, 7055–7058.
[10] H. Wu, J. Yang, J. Šečkutė, N. K. Devaraj, *Angew. Chem. Int. Ed. Engl.* **2014**, *53*, 5805–5809; *Angew. Chem.* **2014**, *126*, 5915–5919.
[11] W. Mao, J. Tang, L. Dai, X. He, J. Li, L. Cai, P. Liao, R. Jiang, J. Zhou, H. Wu, *Angew. Chem. Int. Ed. Engl.* **2021**, *60*, 2393–2397; *Angew. Chem.* **2021**, *133*, 2423–2427.
[12] a) A. M. Courtis, S. A. Santos, Y. Guan, J. A. Hendricks, B. Ghosh, D. M. Szantai-Kis, S. A. Reis, J. V. Shah, R. Mazitschek, *Bioconjugate Chem.* **2014**, *25*, 1043–1051; b) L. D. Lavis, R. T. Raines, *ACS Chem. Biol.* **2008**, *3*, 142–155.
[13] a) A. D. Becke, *J. Chem. Phys.* **1993**, *98*, 5648–5652; b) G. Scalmani, M. J. Frisch, B. Mennucci, J. Tomasi, R. Cammi, V. Barone, *J. Chem. Phys.* **2006**, *124*, 94107.
[14] T. Shen, W. Zhang, P. Yadav, X. W. Sun, X. Liu, *Mater. Chem. Front.* **2023**, *7*, 1082–1092.

Manuscript received: December 21, 2023
Accepted manuscript online: January 19, 2024
Version of record online: ■■, ■■

Communications

Bioorthogonal Chemistry

Y. Deng, T. Shen, X. Yu, J. Li, P. Zou, Q. Gong, Y. Zheng, H. Sun,* X. Liu,* H. Wu* **e202319853**

Tetrazine-Isonitrile Bioorthogonal Fluorogenic Reactions Enable Multiplex Labeling and Wash-Free Bioimaging of Live Cells

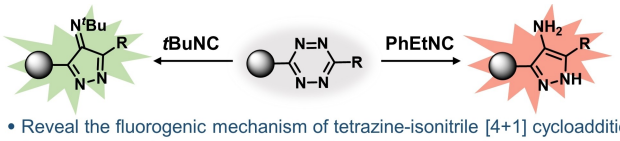

- Reveal the fluorogenic mechanism of tetrazine-isonitrile [4+1] cycloaddition
- Develop highly fluorogenic probe *via* fluorophore in situ formation
- Create mutually orthogonal tools for multicolor cellular no-wash imaging

We developed a series of tetrazine-functionalized bioorthogonal probes for multiplex imaging, by incorporating pyrazole adducts into the fluorophore scaffolds upon click reactions. These modifications are generalizable to various fluorophores, enabling a broad emission range from 473 to 659 nm, and high turn-on ratios up to 3184-fold.